Hindawi Publishing Corporation
Journal of Chemistry
Volume 2013, Article ID 135815, 14 pages
http://dx.doi.org/10.1155/2013/135815

Research Article

Synthesis and Spectroscopic Studies of Axially Ligated Zn(II)5,10,15,20-meso-tetra(p-chlorophenyl)porphyrin with Oxygen and Nitrogen Donors

Gauri D. Bajju, Sujata Kundan, Ashu Kapahi, and Deepmala Gupta

Department of Chemistry, University of Jammu, New Campus, Baba Sahib Ambedkar Road, Jammu&Kashmir, Jammu 180 006, India

Correspondence should be addressed to Gauri D. Bajju; gauribajju@gmail.com

Received 8 December 2011; Revised 8 July 2012; Accepted 9 July 2012

Academic Editor: Franck Rabilloud

Reaction of 5,10,15,20-*meso*-tetra(p-chlorophenyl)porphyrin[H_2(p-Cl)pp] with zinc(II)acetate($Zn(OAc)_2$) and phenols results in the formation of corresponding axially ligated zinc(II)-*meso*-tetra(p-chlorophenyl)porphyrin (X-Zn-t(p-Cl)PP) (X = phenolates and pyridinates). The four-coordinated zinc porphyrin accepts one axial ligand in 1 : 1 molar ratio to form five-coordinated complex, which is purified by column chromatography and characterized by IR spectra, ^{1}H NMR, electronic absorption spectra, elemental analysis, mass spectroscopy, and TGA/DTA studies. IR spectra confirms the appearance of Zn–N_{Por} at 500–400 cm^{-1}, Zn–N_{Py} at 650–570 cm^{-1} and Zn–O at 650–350 cm^{-1}. ^{1}H NMR spectra show that the protons of the Phenolic ring axially attached to the central metal ion are merged with the protons of the tetraphenyl rings of the porphyrin moiety. Absorption spectra reveal that complexes are accompanied by blue shift (hypsochromic shift) for phenolates and red shift (bathchromic shift) for pyridinates in comparison with the basic Zn^{II}porphyrin emission bands. Mass Spectra determine the *m/z* ratio. The percentage of each element is confirmed by elemental analysis. According to the thermal studies, the complexes have a higher thermal stability and the decomposition temperature of these complexes depends on the axial ligation. The *invitro* antifungal activity of the complexes synthesized above had been done by disc diffusion method against the pathogen "*Fusarium spp*.," which shows that with the increase in the concentration of the complexes, the colony diameter decreases and hence percent inhibition increases.

1. Introduction

The chemistry of porphyrins and related compounds dates back to eighteenth century. The porphyrin molecules and their derivatives in different forms are currently utilized in a variety of applications that span medicine (Photodynamic therapy) PDT [1], optoelectronics [2, 3], nanofabrication [4–6], organic chemistry (catalysis) [7], photovoltaics [8], and so on. Metal complexes of tetrapyrollic macrocycles play a key role with respect to life on earth because of their implications in a variety of enzymatic systems [9]. In general, the chemistry of different metalloporphyrins is controlled by the complexed metal and the kind of peripherally and/or axially fixed substituents. These factors influence the electronic density distribution within the core of the macrocycle, and thus determine its reactivity and stability as well. The electronic properties of porphyrins can be changed by introducing suitable substituents at the *meso*-positions or β-position. Synthetic porphyrins, especially *meso*-tetraphenylporphyrin derivatives substituted at the para-positions with soluble acidic, basic and neutral groups are of potential interest in medicinal chemistry because they can form chelates either with some toxic heavy metals or with gamma-ray emitting radioisotopes [10–12]. Substitution with halogens (–F, –Cl, –Br) at *meso*-phenyl position has been shown to enhance catalytic activity [13] and nonlinear optical properties [14]. Also, the phenomenon that metalloporphyrins are coordinated to axial ligands is very common especially in green plant and photosynthetic bacteria, where such coordination impacts a significant effect on both the primary charge separation in the reaction center and energy transfer in antenna systems [15]. This ability of metalloporphyrins to attach additional ligands also determines their role in enzyme and catalytic processes. A great number of experimental results have been

reported over the past three decades concerning the axial ligation properties of these substituted metalloporphyrins with S, O, P, and N bases [16]. Recently, many efforts have been focused on the molecular recognition of biointerest by zinc porphyrins [17, 18]. A binding mode of the pyridine group of the nicotine guest coordinated to the Zn atom of the host was found [19]. The interaction of metalloporphyrins with donor molecules either in their ground or excited states can strongly influence the absorption properties and the efficiency of energy- or electron-transfer processes of porphyrin derivatives [16]. Thus, understanding the effects of axial ligands on the electronic spectra and redox properties of metalloporphyrins is a basic but important subject because of its biological relevance. These investigations have shed light on how axial ligands induce changes in the electronic absorption and other spectral features of zinc(II) derivatives. Generally, the axial coordination of oxygen donors to the metal center represents the supramolecular binding motif. This self-assembly strategy has been successfully applied for the construction of molecular square, coordination polymer and other types of structures [20–22]. It is also known that histidine side chains of proteins have been shown to be important for catalysis in biological systems [23]. Zinc porphyrin cation radicals were extensively studied using an electrochemical EPR technique [24]. The factors affecting the electronic structures of zinc porphyrin cation radical were also examined by Spiro and Coworkers using Resonance Raman Spectra [25] but however, the reactions examined were rather limited.

In the present work, zinc(II)-5,10,15,20-*meso*-tetra(p-chlorophenyl)porphyrin containing different phenolates and pyridinates were synthesized and characterized by various physicochemical techniques. Studies revealed that in these complexes, different phenols and pyridines are bonded at fifth-coordinated site via zinc atom.

2. Experimental

2.1. Materials and Methods. Pyrrole (Fluka, Switzerland) was distilled over potassium hydroxide pellets under reduced pressure before use. *para*-chloro-benzaldehyde is procured from Aldrich, USA and used without further purification. Propionic acid used in the synthesis was obtained from Qualigens (India) and used as such. zinc(II)acetate ($Zn(OAc)_2$) were purchased from E. Merck, India. Silica gel (200–300 mesh) and Silica gel (TLC grade, particle size = 75 μ procured from Merck, Germany) were used for column and thin layer chromatography, respectively. Aluminium oxide (basic type I) purchased from Fluka, Switzerland, was activated at 150°C for at least 24 h [26]. Anhydrous sodium sulphate (Na_2SO_4), potassium carbonate (K_2CO_3), sodium hydrogen carbonate ($NaHCO_3$), sodium hydroxide (NaOH), and calcium chloride ($CaCl_2$) procured from Ranbaxy Labs. Ltd. (India). Chloroform (Merck) was dried over anhydrous calcium chloride at least for three days before use.

2.2. Detection Method. The optical absorption spectra of the compounds were recorded on a Hitachi U-3400, lambda 35 UV-Vis. Spectrophotometer and Elico spectral treats UV-Vis. spectrophotometer using a pair of matched quartz cells of 10 mm path length at an ambient temperature. Absorbance data were obtained as follows. A fixed aliquot of X-Zn^{II}-t(p-Cl)PP (X = phenols and pyridines) was diluted to 2.5 mL giving a total metalloporphyrins concentration of $\sim 4.0 \times 10^{-5}$ M. The oscillator strength (f) of the transitions in absorption spectra were calculated from the expression [27]

$$f = 4.33 \times 10^{-9} \varepsilon \Delta \nu_{1/2}, \quad (1)$$

where ε is the molar absorption coefficient in $dm^3\,mol^{-1}\,cm^{-1}$, and $\Delta\nu_{1/2}$ is the full width at half maximum in cm^{-1}. The ^1H NMR spectra were recorded on a Bruker Avance 400 Ultra shield Spectrometer in $CDCl_3$ using tetramethylsilane (TMS) as internal standard. Porphyrin solutions (0.5 mL) of 10^{-2} to 10^{-3} in $CDCl_3$ were used for ^1H NMR studies. The δ values reported are in ppm with number of protons involved followed by the positions of protons. Inrared spectra were recorded on PERKIN ELMER spectrometer at room temperature in KBr Pellets. In Infrared spectroscopy, the detection of metal-nitrogen (M–N), metal-axial ligand (M–X) vibration and metalloporphyrins with different pure metal isotopes were studied over a large frequency range. The elemental analysis of the precursor H_2-t(p-Cl)PP and its axially ligated zinc(II) derivatives were performed on Elemental Analyzer CHNS-932, LECO, USA at a temperature of about 1000°C using helium as carrier gas and oxygen for combustion. The MALDI mass spectra were recorded on Burker Daltonics spectrophotometer MALDI Data System in positive linear higher power of detection at an accelerating voltage of 20 KV and laser power tuned depending on the sample and the spectra were recorded at room temperature and methanol as solvent. The thermogravimetric analyses (TGA) and differential thermal analyses (DTA) were performed on a Linseis STA PT-1000 in air atmosphere at a heating rate of 10°C/min. Antifungal activity of the complexes has been done by disc-diffusion method against the pathogen "*Fusarium spp.*"

5,10,15,20-meso-tetra(p-chlorophenyl)porphyrin[H_2t(p–Cl)PP]. The preparation of H_2t(p–Cl)PP was carried out by the condensation of pyrrole with p-chlorobenzaldehyde in refluxing propionic acid [28–30]. H_2t(p–Cl)PP prepared was purified by column chromatography using $CHCl_3$ as eluent. UV-Vis (λ_{max}(nm)) (MtOH/$CHCl_3$) (2.5%,v/v): 425.5, 519, 559, 599.5, 653.2; ^1H NMR ($CDCl_3$) (δ, ppm): −2.93(S,2H,N–H), 8.89(S,8H,β-pyrrole), 8.25(d,8H,H_o), 7.75(d,8H,H_m); IR Spectra (in KBr): ν(N–H) at 3499 cm^{-1}, ν(C–H) at 2966 cm^{-1}, ν(C–N) at 1340 cm^{-1}, ν(C=C) at 1591 cm^{-1}, ν(C–N) at 2342 cm^{-1}, ν(C–Cl) at 798.7 cm^{-1}; CHN: Anal. Calcd. (%), $C_{44}H_{26}N_4Cl_4$: C = 70.15; H = 3.45; N = 7.44. Found: C = 70.29; H = 3.52; N = 7.46.

Zinc(II)5,10,15,20-meso-tetra(p-chlorophenyl)porphyrin[Zn(II)-t(p–Cl)PP]. $Zn(OAc)_2{\cdot}2H_2O$(37 mg, 0.17 mmol) in methanol (10 mL) and 5,10,15,20-meso-tetra(p-chlorophenyl)porphyrin (50 mg, 0.056 mmol) dissolved in chloroform (10 mL) were taken in a 250 mL conical flask. The

reaction mixture was stirred at about 60–70°C for 2-3 h. The colour instantly changed to reddish purple, and the solution became homogeneous. After completion, the solution was dried over anhydrous sodium sulphate and reduced in vacuo. Redissolve the resulting solid in a minimum amount of hot chloroform (50 mL). Purify on a silica column eluting with chloroform. The Zn^{II}-t(p–Cl)PP band should be reddish purple and elute first. The yield was 52 mg (98%). UV-Vis (CH_2Cl_2) (λ_{max} (nm)): 423, 549, 588; ^{1}H NMR ($CDCl_3$): 8.93(S,8H,β-pyrrole-H), 8.20(d,8H,Ar-H), 7.74(m,10H); IR Spectra (in KBr): ν(C–H) at 2966.2 cm^{-1}, ν(C–Cl) at 798.3 cm^{-1}, ν(Zn–N_{Por}) at 470 cm^{-1}; CHN: Anal. Calcd. (%), $C_{44}H_{24}N_4Cl_4Zn$: C = 64.59; H = 2.93; N = 6.85. Found: C = 64.50; H = 2.94; N = 6.70.

Zinc(II)5,10,15,20-meso-tetra(p-chlorophenyl)porphyrin-phenoxide[X-Zn(II)-t(p-Cl)PP]

$$\text{Zn (II) -t(p-Cl) PP} + \text{X} \rightleftarrows \text{X-Zn (II) -t(p-Cl) PP} \quad (2)$$

Zinc(II)5,10,15,20-meso-tetra(p-chlorophenyl)porphyrin (6.602×10^{-4} moles; 0.564 g) in 15 mL of $CHCl_3$ and phenol (X) (3.086×10^{-2} moles) in methanol was refluxed for 1 hour. After concentrating, the reaction mixture was extracted with 2 N NaOH solution and chloroform as an eluent. The compound recovered after extraction was passed through Na_2SO_4. The solvent was recovered under reduced pressure and chromatographed through basic alumina using chloroform as an eluent, recrystallized with Petroleum ether, and characterized by UV-visible and ^{1}H NMR spectra. The colour of the complex formed depends upon the nature of axially ligated phenols (Scheme 2(a)).

Zinc(II)5,10,15,20-meso-tetra(p-chlorophenyl)porphyrin-pyridine[X-Zn(II)-t(p-Cl)PP]

$$\text{Zinc Porphyrin} + \text{Pyridine} \leftrightarrows \text{Zinc Porphyrin pyridinate} \quad (3)$$

Pyridine (3.211×10^{-2} moles) (X) and [Zn-t(p-Cl)PP] in 1 : 1 molar ratio were stirred without heating. After completion of reaction as again indicated by TLC, the reaction mixture is extracted with distilled water. The extracted portion containing compound was evaporated by vacuum pump, and the dried product was then dissolved in chloroform and filtered through anhydrous sodium sulphate and evaporated by vacuum pump. The purification of the product was done by column chromatography through basic alumina using chloroform as the eluent. The dried product was crystallized with chloroform and recrysatllized with petroleum ether. Finally, the compound was characterized by UV-Vis and ^{1}H NMR spectra (Scheme 2(b)).

3. Results and Discussion

3.1. Infrared Spectroscopy. Vibrational wave numbers are frequently used in the elucidation of the relative strength of interaction between the metal and the ligand and are affected by their oxidation state and mode of bonding between them. The IR Spectra of free base porphyrin(H_2-t(p-Cl)PP) and its axially ligated zinc(II) metal derivatives containing the -Cl group at *meso*-phenyl position showing strong absorption band at 798 cm^{-1} (800–600 cm^{-1}) agree well within the literature [31, 32]. The IR absorption spectra of (H_2-t(p-Cl)PP) and their corresponding axially ligated Zn(II)acetate$(OAc)_2$ with different phenolates and pyridinates as axial ligand is shown in (Table 1). The metallation of porphyrin was confirmed by the absence of vibrational frequencies occurring due to imino groups of the porphyrin ring and the appearance of Zn–N_{Por} band in the range of 500–400 cm^{-1}. The incorporation of various phenolates and pyridinates in (X-Zn-t(p-Cl)PP) (X = different phenolates and pyridinates as axial ligands) was confirmed by the appearance of Zn–O and Zn–N_{Py} vibrational frequencies in the range of 650–350 cm^{-1} and 650–570 cm^{-1}, respectively. The axially ligated Zn^{II} derivatives cause a slight variation in the value of vibrational frequencies. For example, In the spectra p-NH_2phO-Zn-t(p-Cl)PP (Figure 1), aromatic ν(C–H) at 2964.1 cm^{-1}, ν(C–N) at 1351.6 cm^{-1}, ν(C=C) at 1590 cm^{-1}, ν(C=N) at 2360 cm^{-1}, ν(C–O) at 1207 cm^{-1}, ν(C–Cl) at 799.3 cm^{-1}, ν(Zn–N_{Por}) at 482 cm^{-1}, and ν(Zn–O) at 496.3 cm^{-1}. An additional vibrational stretching frequency due to -NH_2 group of phenol lies at 3298 cm^{-1} and 3371 cm^{-1} for $\nu(NH_2)_{sym}$ and $\nu(NH_2)_{asym}$, respectively. On comparing this complex with p-NH_2py-Zn-t(p-Cl)PP (Figure 2), aromatic ν(C–H) at 2965 cm^{-1}, ν(C–N) at 1094 cm^{-1}, ν(C=C) at 1652 cm^{-1}, ν(C=N) 2354 cm^{-1}, ν(C–Cl) at 798.6 cm^{-1}, ν(Zn–N_{Por}) at 495 cm^{-1}, ν(Zn–N_{Py}) at 618 cm^{-1}. Again for this complex, additional vibrational stretching frequencies for $(NH_2)_{sym}$ and $\nu(NH_2)_{asym}$ appear at 3280 cm^{-1} and 3450 cm^{-1}, respectively. The other vibrational frequencies as in case of p-OCH_3phO-Zn-t(p-Cl)PP (see, Supplementary Material: Figure A1 available online at doi: 10.1155/2013/135815) are attributed to the vibrational stretching frequency of the methoxy group as subsituent at the para position of the phenyl ring of the phenol axially ligated via zinc atom.

3.2. ^{1}H NMR Spectroscopy. ^{1}H NMR was widely used as an analytical tool and the new structural insights that resulted were a major reason for the revival of interest in porphyrins chemistry. The ^{1}H NMR spectra of the p-chloro-*meso*-tetraphenylporphyrin and their Zn(II) derivatives containing different phenolates and pyridinates as axial ligand are highly characteristic and establish the structural integrity of these compounds in solution and data accumulated in Table 2. The ^{1}H NMR spectra of free-base porphyrins (H_2TPP) give three characteristic proton resonances: (a) β-pyrrole protons, (b) imino protons, and (c) *meso*-aryl protons. The substituent in β-positions and peripheral phenyl groups alters these proton resonances. The integrated intensity of the resonances agrees well with the number of protons. The presence of electron-withdrawing chloro group at the para position of the *meso*-phenyl ring causes a slight deshielding effect of the β-pyrrole protons resulting in a

Table 1: Main Infrared absorption frequencies corresponding to various groups in [X-Zn^{II}-t(p-Cl)PP] [X = phenolates and pyridinates].

Entry	Compound	ν (N–H) (cm^{-1})	ν (C–H) (cm^{-1})	ν (C–N) (cm^{-1})	ν (C=C) (cm^{-s1})	ν (C–O) (cm^{-1})	ν (C=N) (cm^{-1})	ν (C–Cl) (cm^{-1})	ν (Zn–N_{Por}) (cm^{-1})	ν (Zn–N_{Py}) (cm^{-1})	ν (Zn–O) (cm^{-1})	Other assignments
1	H_2t(p-Cl)PP	3499	2966	1340	1591	—	2342	798.7	—	—	—	
2	Zn-t(p-Cl)PP	—	2966.2	1341.1	1589.6	1207.5	2347	798.3	470	—	—	
3	phO-Zn-t(p-Cl)PP	—	2960.4	1350.3	1584.1	1206.5	2339.3	798.9	474	—	500.7	
4	p-OCH_3phO-Zn-t(p-Cl)PP	—	2962.7	1337.7	1590	1207.2	2342	800.1	489	—	496.2	ν(C–H) = 2851.1 $\nu(C–O–C)_{sym}$ = 1020.2 $\nu(C–O–C)_{asym}$ = 1261.3
5	p-NH_2 phO-Zn-t(p-Cl)PP	—	2964.1	1351.6	1589.2	1205	2360	799.3	482	—	496.3	$\nu(NH_2)_{sym}$ = 3298 $\nu(NH_2)_{asym}$ = 3371
6	p-NO_2 phO-Zn-t(p-Cl)PP	—	2963	1351.4	1590	1207.3	2360	798.7	471	—	496.3	$\nu(NO_2)_{sym}$ = 1345 $\nu(NO_2)_{asym}$ = 1520
7	p-CH_3py-Zn-t(p-Cl)PP	—	2964	1095	1640	—	2350	799.5	492	617	—	$\nu(CH_3)$ = 2920
8	p-NH_2py-Zn-t(p-Cl)PP	—	2965	1094	1652	—	2354	798.6	495	618	—	$\nu(NH_2)_{sym}$ = 3280 $\nu(NH_2)_{asym}$ = 3450
9	p-CNpy-Zn-t(p-Cl)PP	—	2964.0	1096.1	1636.7	—	2358	796	490	617.4	—	ν(CN) = 2280

Table 2: ^{1}H NMR data of free base H_2-t(p-Cl)PP and axially ligated Zn^{II}-t(p-Cl)PP showing chemical shift (δ in ppm) values in $CDCl_3$ at 298 K.

Porphyrins	β-Pyrrole protons	Imino protons	Meso-aryl protons	Other protons
H_2t(p-Cl)PP	8.89 (S)	−2.93 (S)	8.25 (d, 8H, H_o) 7.75 (d, 8H, H_m)	
Zn-t(p-Cl)PP	8.93 (S, 8H)	—	8.20 (d, 8H) 7.74 (m, 10H)	
phO-Zn-t(p-Cl)PP	8.54 (S, 8H)	—	8.29 (d, 8H, H_o) 7.80 (d, 8H, $H_{m,P}$)	
p-OCH_3phO-Zn-t(p-Cl)PP	8.92 (S, 8H)	—	8.26 (d, 8H, H_o) 7.78 (d, 8H, $H_{m,P}$)	3.8 (S, 3H, H_{ome})
p-NH_2phO-Zn-t(p-Cl)PP	8.95 (S, 8H)	—	8.27 (d, 8H, H_o) 7.79 (d, 8H, $H_{m,P}$)	5.6 (S, 2H, H_{NH2})
p-CH_3phO-Zn-t(p-Cl)PP	9.2 (S, 8H)	—	8.21 (d, 8H, H_o) 7.7 (d, 8H, $H_{m,P}$)	2.7 (S, 3H, H_{me})
p-NO_2phO-Zn-t(p-Cl)PP	8.18 (S, 8H)	—	8.23 (d, 8H, H_o) 7.60 (d, 8H, $H_{m,P}$)	
p-CH_3py-Zn-t(p-Cl)PP	8.12 (S, 8H)	—	8.26 (d, 8H, H_o) 7.96 (d, 8H, $H_{m,P}$)	2.6 (S, 3H, H_{me})
p-NH_2py-Zn-t(p-Cl)PP	8.27 (S, 8H)	—	8.16 (d, 8H, H_o) 7.46 (d, 8H, $H_{m,P}$)	5.4 (S, 2H, H_{NH2})
p-CN-py-Zn-t(p-Cl)PP	8.25 (S, 8H)	—	8.05 (d, 8H, H_o) 7.29 (d, 8H, $H_{m,P}$)	

δ in ppm, the nature of splitting pattern (S) (S: Singlet, d: doublet, t: triplet, m: multiplet), number of proton (s) and their location in the porphyrins respectively are given in parenthesis; o: ortho; p: para; m: meta.

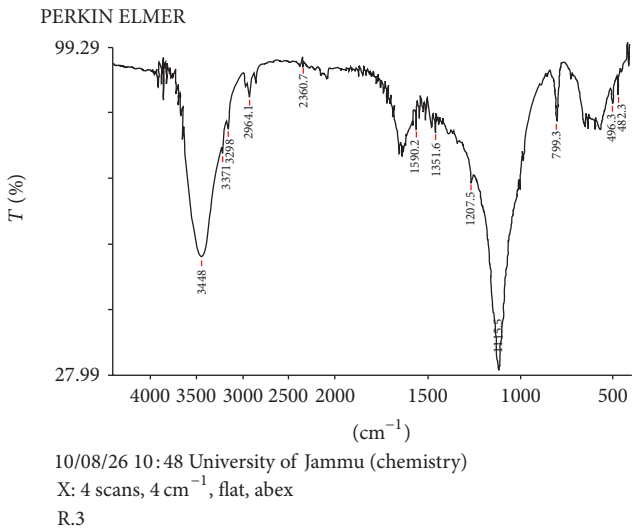

Figure 1: IR spectra of p-NH_2phO-Zn-t(p-Cl)PP.

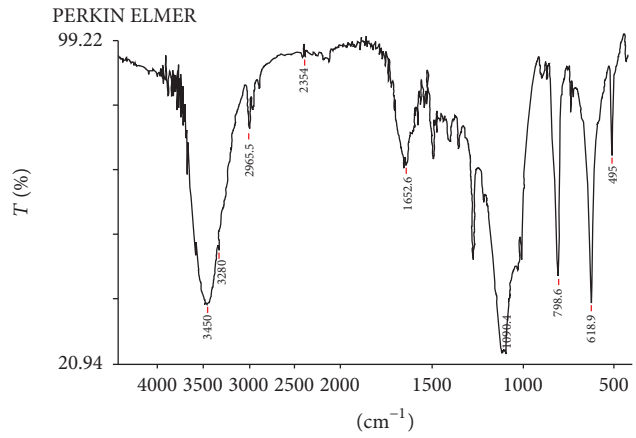

Figure 2: IR spectra of p-NH_2py-Zn-t(p-Cl)PP.

slight downfield shift of *meso*-substituted porphyrins relative to simple *meso*-tetraphenylporphyrin (H_2TPP) [33]. This shielding and deshielding of the β-pyrrole protons is most likely a consequence of meso –C–C– dihedral angle much greater than 0°, thereby placing the β-pyrrole protons in a more shielded/deshielded environment produced by the anisotropic effect of substituent ring current. The inner imino protons of the H_2TPP resonate at −2.79 ppm, while those of H_2-t(p-Cl)PP appear at −2.93 ppm, this peak however disappeared in metallated Zn^{II} porphyrin because the two H-atoms are replaced by Zn metal ion. This is a great movement to high field on the basis of strong shielding effect of porphyrin ring. The *meso*-aryl protons of H_2TPP resonates as a singlet at 8.19 ppm of ortho and 7.59 ppm of meta and para protons, respectively, and are shifted marginally depending upon the nature of the substituents

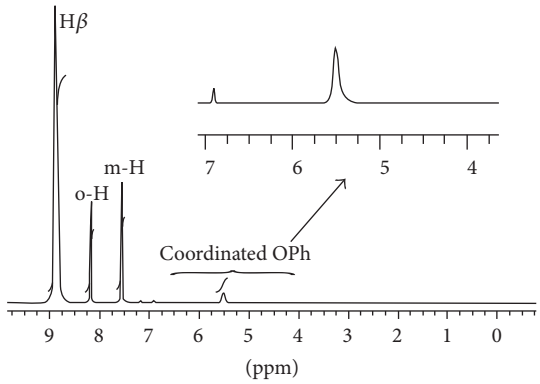

Figure 3: ^{1}H NMR spectra p-NH_2phO-Zn-t(p-Cl)PP in $CDCl_3$ at 298 K.

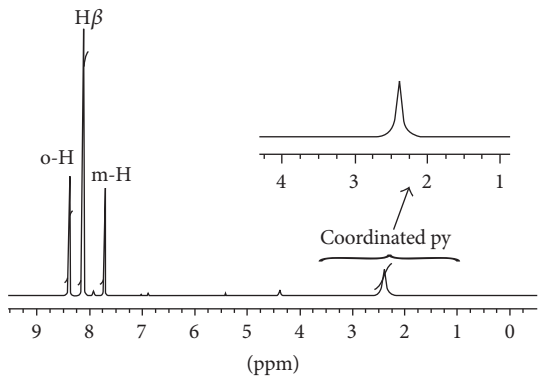

Figure 4: ^{1}H NMR spectra p-CH_3py-Zn-t(p-Cl)PP in $CDCl_3$ at 298 K.

attached at the *meso*-phenyl position as in case of H_2-t(p-Cl)PP, for which the resonance occurs at at 8.25 ppm of ortho and 7.75 ppm of meta protons, that is, resonance is shifted downfield relative to H_2TPP. In axially ligated zinc compounds of H_2-t-(p-Cl)PP, a slight difference in the proton resonance is observed depending upon the nature of ligand axially ligated (Table 2). The ^{1}H NMR spectra of p-NH_2phO-Zn-t(p-Cl)PP (Figure 3), indicates that the β-pyrrole protons resonate as a singlet at 8.95 ppm, the *meso*-aryl ortho protons resonate as duplet at 8.27 ppm and *meso*-aryl meta and para protons resonate as duplet at 7.79 ppm, respectively. The amino protons of para-amino phenolate axially ligated via zinc atom resonate as duplet at 5.6 ppm, which is downfield (deshielded) with respect to p-NH_2py-Zn-t(p-Cl)PP (Figure 4). In case of p-NH_2py-Zn-t(p-Cl)PP, the β-pyrrole protons resonate as a singlet at 8.27 ppm, the *meso*-aryl ortho protons resonate as duplet at 8.16 ppm, and *meso*-aryl meta and para protons resonate as duplet at 7.46 ppm, respectively. The amino protons of para-amino pyridinate resonate as singlet at 5.4 ppm, which is upfield (shielded). Thus, for p-NH_2py-Zn-t(p-Cl)PP resonance of protons occur slightly upfield with respect to p-NH_2phO-Zn-t(p-Cl)PP because shielding power of nitrogen is more than oxygen due to its less electronegative value than oxygen and hence display spectra towards upfield.

3.3. Absorption Spectroscopy. The optical absorption spectrum is an important phenomenon to distinguish between the free base porphyrins and their metalloderivatives based on profound theoretical analysis of the experimental and quantum-chemical data of the previously mentioned monograph [34]. According to this interpretation the absorption spectra of porphyrins do not exhibit bands of $n \rightarrow \pi^*$ transitions because of the symmetry of the n orbitals and anti symmetry of the n orbitals with respect to the plane of the porphyrin molecule. All bands are of $\pi \rightarrow \pi^*$ origin. The Soret band is due to an electronic $^1A_{1g} \rightarrow {}^1E2_u$ transition to the highest energy vacant π^* orbital. In substituted porphyrins $E2_u$ is split into two states $B2_{2u}$ and $B2_{3u}$ which are close in energy, as a result of the reduced symmetry of the π-electron cloud. The electronic transitions to state $E2_u$ (or $B2_{2u}$ and $B2_{3u}$) are allowed, therefore the intensity of the Soret band is always very high ($\varepsilon = 10^5$). Bands I and III of the visible region belong to quasi-forbidden electronic transitions. The reasons for transitions $^1A_{1g} \rightarrow B2_{3u}$ and $^1A_{1g} \rightarrow B2_{2u}$ being allowed, which is responsible for the appearance of band I and III. Bands II and IV are of vibrational origin, that is they are vibrational satellites of bands II and III, respectively. A factor that must be considered in the interpretation of the spectra in the visible and ultraviolet region is that the phenyl and substituted phenyl rings cannot be coplanar with the porphine nucleus. Examination of molecular models indicates that the four benzene rings have partial rotations that cannot bring them within 60° of being coplanar with the resonating porphine system. Since the average angle of the attached rings is probably considerably greater than this is apparent that resonance interactions between two aromatic systems must be greatly reduced from what would be expected if they were coplanar. Hence, the bathochromic shifts and spectral intensifications observed are considerably less than what would be expected in simpler aromatic systems with greater freedom of rotation. Generally, the absorption spectra of Zn(II)porphyrins are quite "normal" in that they exhibit the expected B and Q bands. The optical absorption spectral data of Zn(II) metal derivatives containing different phenolates and pyridinates as axial ligand in chloroform is shown in Table 3. The absorption spectra of H_2t(p-Cl)PP exhibit the typical Soret band at 425.5 nm and four Q-bands, that is, $Q_y(1,0)$, $Q_y(0,0)$, $Q_x(1,0)$, and $Q_x(0,0)$ at 519 nm, 559 nm, 599.5 nm, and 653.2 nm, respectively. On metallation, the porphyrin ring deprotonates forming dianionic ligand. The metal ions behaved as Lewis acids accepting lone pairs of electrons from dianionic porphyrin ligands. Unlike most transition-metal complexes, their colour is due to absorption(s) within the porphyrin ligands involving the excitation of electrons from π to π^* porphyrin ring orbital [35]. Therefore, all bands are of $\pi \rightarrow \pi^*$ origin. Since, the porphyrin ring belongs to the D_{2h} point group, the number of peaks in UV-visible spectra were decreased when Zn(II) ion inserted into the porphyrin because the metalloporphyrin belongs to the D_{4h}-point group. The position and intensity of the absorption bands in UV-vis spectra varies with the nature of the substituted axial ligands. It is of interest

Table 3: Optical absorption data of X-Zn^{II}-t(p-Cl)PP (X = phenolates and pyridinates as axial ligands) in $CHCl_3$ showing λ_{max} together with log ε and $\nu_{1/2}$.

Compound	B-bands λ_{max}, (log ε), $\nu_{1/2}$ (nm), (M^{-1} cm^{-1}), (cm^{-1})	Q-bands λ_{max}, (log ε), $\nu_{1/2}$ (nm), (M^{-1} cm^{-1}), (cm^{-1})
H_2t(p-Cl)PP	425.5	519, 559, 599.5, 653.2
Zn-t(p-Cl)PP	423	549, 588
phO-Zn-t(p-Cl)PP	418.5, (5.98), 672	548, (4.69), 839 586, (3.06)
α-Naphthol-Zn-t(p-Cl)PP	416.4, (4.76), 670	545, (4.32), 835 584, (3.02)
o-OCH_3phO-Zn-t(p-Cl)PP	418, (4.72), 831	548, (4.09), 719 589, (3.35)
m-OCH_3ph-Zn-t(p-Cl)PP	416, (4.70), 831	548, (4.09), 719 589, (3.37)
p-OCH_3phO-Zn-t(p-Cl)PP	417, (4.68), 839	549, (4.16), 724 591, (3.31)
o-CH_3phO-Zn-t(p-Cl)PP	416, (4.92), 682	544, (4.61), 732 580, (3.01)
m-CH_3phO-Zn-t(p-Cl)PP	416, (4.83), 684	543, (4.54), 729 583, (3.17)
p-CH_3phO-Zn-t(p-Cl)PP	416, (485), 684	544, (4.61), 732 581, (3.03)
o-NH_2phO-Zn-t(p-Cl)PP	420, (4.82), 849	549, (4.64) 591, (3.56)
p-NH_2phO-Zn-t(p-Cl)PP	420, (4.82), 851	546, (4.61) 589, (3.40)
o-CH_3py-Zn-t(p-Cl)PP	424.3, (4.70), 882	556.3, (4.27), 849 601.6, (4.16)
m-CH_3py-Zn-t(p-Cl)PP	424.5, (4.89), 889	556.8, (4.31), 846 602.7, (4.22)
p-CH_3py-Zn-t(p-Cl)PP	424.8, (4.96), 895	557.1, (4.42), 839 602.9, (4.36)
o-NH_2py-Zn-t(p-Cl)PP	425.3, (4.808), 885	558.1, (4.29), 845 607.9, (4.17)
m-NH_2py-Zn-t(p-Cl)PP	425.5, (4.825), 889	559.2, (4.29), 851 609.2, (4.11)
p-NH_2py-Zn-t(p-Cl)PP	425.6, (4.84), 897	559.9, (4.31), 862 609.6, (4.13)

to note that among the different ligands attached to the metal ion, oxygen donors have blue shift (hypsochromic shift) of B and Q bands whereas nitrogen donors have broadened Soret and visible bands, which are slightly red-shift (Bathochromic shift) relative to their free-base metal porphyrins. This unusual Red/blue shift and changes in the absorption bands could be explained on the basis of four-orbital approach of Gouterman [36]. When a comparative study of optical absorption spectral data of p-CH_3phO-Zn-t(p-Cl)PP (see, Supplementary Material: Figure A2(c)), in chloroform is done with respect to p-CH_3py-Zn-t(p-Cl)PP (see, Supplementary Material: Figure A2(d)), a slight red shift, that is, to longer wavelength was observed for p-CH_3py-Zn-t(p-Cl)PP because pyridine (nitrogen donors) which are basic in nature and the nonbonding electron pair present on the heteroatom nitrogen are free to donate, therefore, require lesser energy for transition and are red shifted whereas in case of phenols (oxygen donors) which are acidic in nature and the phenyl ring present in phenol is electron withdrawing which attracts the lone pair of electrons present on the oxygen, thereby, reduce the tendency to donate the electron and therefore, require higher energy for transition and are blue shifted. Thus, ZnTPP preferentially binds "hard" ligands with donor atoms that have relatively

Table 4: Optical absorption data of X-Zn^{II}-t(p-Cl)PP (X = phenolates and pyridinates as axial ligands) in different solvents at different concentration.

Compound	Solvent	B band at different concentration λ_{max} (nm), $\nu_{1/2}$ (cm^{-1}) (Abs.), ε (M^{-1} cm^{-1})			Q band at different concentration λ_{max} (nm), $\Delta\nu_{1/2}$ (cm^{-1}) (Abs.), ε (M^{-1} cm^{-1})			Oscillator strength (f) = $4.33 \times 10^{-9} \varepsilon \Delta\nu_{1/2}$					
								B-band			Q-band		
		10^{-3}	10^{-4}	10^{-5}	10^{-3}	10^{-4}	10^{-5}	10^{-3}	10^{-4}	10^{-5}	10^{-3}	10^{-4}	10^{-5}
4-NH_2PhO-Zn-t(P-Cl)PP	MtOH	425, 698 (0.536), 45792	425, 698 (0.709, 60572)	424, 909 (0.999), 8.5427	558, 650 (0.999),85364 596 (0.697)	556, 744 (0.400),34183 584 (0.158)	563, 460 (0.279), 2.38579 584 (0.421)	0.1383989	0.1836092	0.0000336	0.2402569	0.1101212	0.00000475
	CH_2Cl_2	423, 861 (0.241), 20589	422, 865 (0.400), 34173	422, 881 (0.791), 6.76404	552, 541 (0.999), 85364 589 (0.891)	552, 814 (0.758), 64776 580 (0.400)	552, 814 (0.762), 6.5160 578 (0.419)	0.07676	0.127993	0.0000258	0.1999677	0.2283108	0.0000229
	$CHCl_3$	420, 874 (0.298), 25459	419, 931 (0.536), 45792	419, 931 (0.702), 6.00298	540, 597 (0.601), 51355 574 (1.054)	542, 845 (0.959), 81953 570 (0.839)	540, 565 (0.441), 3.7711 568 (0.249)	0.0963475	0.1845981	0.0000242	0.1327532	0.2998537	0.00000922
	C_6H_6	416, 890 (0.599), 51177	414, 844 (0.786), 67151	414, 844 (0.959), 8.20065	540, 565 (0.839), 71693 563 (0.702)	543, 559 (0.554), 47343 569 (0.298)	543, 559 (0.641), 5.4814 567 (0.536)	0.197221	0.245405	0.0000299	0.1753933	0.1145923	0.0000133
2,4-Cl_2PhO-Zn-t(P-Cl)PP	MtOH	435, 1010 (0.383), 38157	432, 1025 (0.500), 47866	432, 1073 (0.573), 5.48549	551, 574 (0.746), 71411 574 (0.008)	546, 710 (0.968), 92669 574 (0.624)	543, 717 (0.886), 8.4819 571 (0.446)	0.1774863	0.21244137	0.0000255	0.1774863	0.2848923	0.0000263
	CH_2Cl_2	433, 1068 (0.414), 39629	431, 979 (0.863), 82617	431, 1078 (0.983), 9.41054	547, 707 (0.999), 95629 576 (0.729)	546, 710 (0.968), 92669 573 (0.564)	546, 679 (0.868), 8.3096 572 (0.446)	0.1832619	0.3502192	0.0000439	0.2927500	0.2848923	0.0000244
	$CHCl_3$	432, 926 (0.371), 35513	431, 1025 (0.588), 56290	431, 1029 (0.798), 7.63948	543, 591 (0.582), 55712 576 (0.386)	542, 561 (0.434), 41548 568 (0.221)	542, 529 (0.649), 6.2131 565 (0.430)	0.1423922	0.24982909	0.0000340	0.1425687	0.1009255	0.0000142
	C_6H_6	429, 1138 (0.482), 46139	429.4, 1066 (0.500), 47866	429.2, 1077 (0.689), 6.59599	540, 565 (0.542), 51883 563 (0.466)	538, 602 (0.799), 76491 567 (0.443)	536.8, 578 (0.732), 7.0076 563 (0.448)	0.2273518	0.2209389	0.0000307	0.1269292	0.1993860	0.0000175
2-NH_2Py-Zn-t(P-Cl)PP	MtOH	429, 1088 (0.279), 23645	427, 1098 (0.783), 66359	426, 1153 (0.901), 7.63602	585, 483 (0.347), 29395 611 (0.295)	582, 516 (0.645), 54644 609.4 (0.412)	580.4, 646 (0.498), 2.5256 605 (0.258)	0.1113925	0.3154932	0.0000381	0.0614764	0.1220899	0.00000706
	CH_2Cl_2	428, 1142 (0.999), 84666	427, 1098 (0.924), 78309	427, 1098 (0.961), 8.14451	552, 541 (0.402), 34054 579 (0.378)	551.7, 520 (0.627), 53119 576 (0.494)	550, 545 (0.743), 6.2969 574 (0.496)	0.41866151	0.3723076	0.0000387	0.0797725	0.1196027	0.0000148
	$CHCl_3$	425, 1108 (0.589), 49918	423, 1169 (0.959), 81276	422, 1123 (0.772), 6.54273	548, 674 (0.501), 42441 577 (0.324)	547.2, 575 (0.501), 42444 575 (0.349)	547, 582 (0.447), 3.7883 574 (0.248)	0.2394886	0.4114004	0.0000318	0.1238606	0.1056749	0.00000955
	C_6H_6	420, 1134 (0.740), 62715	421, 1025 (0.497), 42120	420, 1185 (0.589), 4.99180	542, 593 (0.662), 56079 576 (0.472)	541, 595 (0.461), 39055 578 (0.362)	539, 404 (0.689), 5.8393 575 (0.532)	0.3079444	0.1869391	0.0000256	0.1439939	0.1006193	0.00001021

Table 5: Elemental analytical data of X-Zn^{II}-t(p-Cl)PP (X = phenolates and pyridinates as axial ligand) along with their calculated values.

Compound	Calculated percentage			Found percentage		
	C	H	N	C	H	N
phO-Zn-t(p-Cl)PP [$(C_6H_5O)Zn(C_{44}N_{24}N_4Cl_4)$]	65.90	3.18	6.14	66.76	3.24	6.23
p-NH_2phO-Zn-t(p-Cl)PP [$(C_6H_7NO)Zn(C_{44}N_{24}N_4Cl_4)$]	64.72	3.34	7.54	65.19	3.39	8.25
p-NO_2phO-Zn-t(p-Cl)PP [$(C_6H_5NO_3)Zn(C_{44}N_{24}N_4Cl_4)$]	62.80	3.03	7.32	63.40	3.09	7.39
2,4-Cl_2phO-Zn-t(p-Cl)PP [$(C_6H_4Cl_2O)Zn(C_{44}N_{24}N_4Cl_4)$]	61.22	2.75	5.70	61.27	2.77	5.72
p-OCH_3phO-Zn-t(p-Cl)PP [$(C_7H_8O_2)Zn(C_{44}N_{24}N_4Cl_4)$]	65.04	3.29	5.70	65.35	3.33	5.98
o-NH_2py-Zn-t(p-Cl)PP [$(C_5H_6N_2)Zn(C_{44}N_{24}N_4Cl_4)$]	64.52	3.28	9.20	65.22	3.35	9.31
p-CH_3py-Zn-t(p-Cl)PP [$(C_6H_7N)Zn(C_{44}N_{24}N_4Cl_4)$]	65.90	3.40	7.68	66.05	3.43	7.70

Table 6: Mass data for X-Zn^{II}-t(p-Cl)PP (X = phenolates and pyridinates as axial ligand).

Compound	Formula	*m/z* ratio	
		Observed	Calculated
phO-Zn-t(p-Cl)PP [$(C_6H_5O)Zn(C_{44}N_{24}N_4Cl_4)$]	$C_{50}H_{29}N_4Cl_4ZnO_1$	911.6	911.18
p-NH_2phO-Zn-t(p-Cl)PP [$(C_6H_7NO)Zn(C_{44}N_{24}N_4Cl_4)$]	$C_{50}H_{31}N_5Cl_4ZnO_1$	926.6	927.8
p-NO_2phO-Zn-t(p-Cl)PP [$(C_6H_5NO_3)Zn(C_{44}N_{24}N_4Cl_4)$]	$C_{50}H_{29}N_5Cl_4ZnO_3$	956.11	956.19
2,4-Cl_2phO-Zn-t(p-Cl)PP [$(C_6H_4Cl_2O)Zn(C_{44}N_{24}N_4Cl_4)$]	$C_{50}H_{27}N_4Cl_6ZnO_1$	980.2	980.8
p-OCH_3phO-Zn-t(p-Cl)PP [$(C_7H_8O_2)Zn(C_{44}N_{24}N_4Cl_4)$]	$C_{51}H_{31}N_4Cl_4ZnO_2$	941.3	941.22
o-NH_2py-Zn-t(p-Cl)PP [$(C_5H_6N_2)Zn(C_{44}N_{24}N_4Cl_4)$]	$C_{49}H_{30}N_6Cl_4Zn$	911.4	912.08
p-CH_3py-Zn-t(p-Cl)PP [$(C_6H_7N)Zn(C_{44}N_{24}N_4Cl_4)$]	$C_{50}H_{31}N_5Cl_4Zn$	911.2	911.6

high electronegativities and low polarizabilities such as N or O donor ligands while ligands with less electronegative, more polarizable donor atoms such as S, P, or unsaturated N cause a larger red shift because they allow negative charge to be transferred to the porphyrin ring. When the optical absorption spectra of axially ligated Zn-t(p-Cl)PP is recorded in different solvents (Table 4) and the spectra of p-NH_2phO-Zn-t(p-Cl)PP is displayed in (Figure 5), which shows only marginal changes in λ_{max} values, absorption coefficient (ε) and oscillator strength (f) values are observed. The data also reveal that a change in polarity of the solvent does not significantly alter the position of the transition but there is a significant increase in "Fwhm" ($\upsilon_{1/2}$) and "f" values of transitions by increasing the polarity of the solvent. In polar solvents such as methanol, ethanol, CH_2Cl_2, and $CHCl_3$, the π-π^* bands undergo red shifts. This is so since excited state is more polar than the ground state and hence stabilization is greater relative to the ground state in polar solvents but as we move from polar to nonpolar solvents such as benzene, toluene, and CCl_4, however, the complexes usually displayed a spectral drift for a period of time. It is observed that for all the axially ligated Zn(II) derivatives, B and Q bands exhibit a red shift on increasing the polarity of the solvents in the order: MtOH > CH_2Cl_2 > $CHCl_3$ > benzene (Table 4). For example, in case of p-NH_2phO-Zn-t(p-Cl)PP (Figure 5), λ_{max} values in MtOH were observed at 425, 596, and 558 nm, respectively, while in benzene, the λ_{max} values were observed at 416, 546, and 540 nm, respectively. However, both B(0,0) and Q(0,0) exhibits only a small change in the f values. The magnitude of change of the "f" values in axially ligated Zn(II) metal derivatives of porphyrins reveal the relative strength of $\pi \rightarrow \pi^*$ interaction.

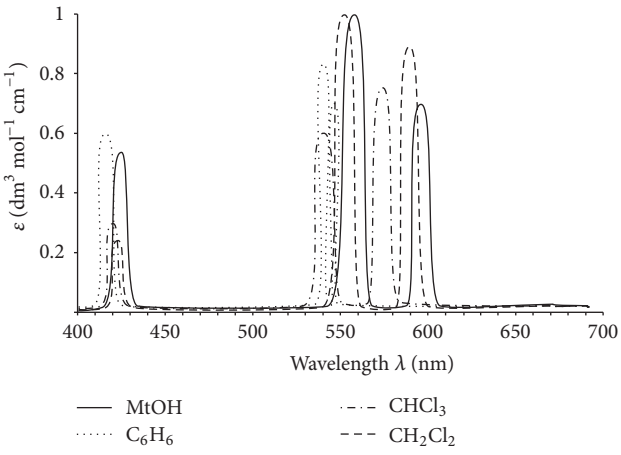

Figure 5: Optical absorption spectra of p-NH_2phO-Zn-t(p-Cl)PP in different solvents.

3.4. Elemental Analysis. The purity of Zn(II) metal derivatives of 5,10,15,20-meso-tetra(p-chlorophenyl)porphyrin containing different phenolates and pyridinates as axial ligand are also characterized by their elemental analysis and data is accumulated in Table 5.

3.5. Mass Spectroscopy. Mass spectroscopy is a key analytical method for qualitatively identifying the different porphyrinic forms. The MALDI mass [37] spectral data of axially ligated zinc(II) metal derivative containing different phenolates and pyridinates as axial ligand is accumulated in Table 6.

Table 7: *In vitro* efficacy of axially ligated Zn^{II}-t(p-Cl)PP complexes against "Fusarium spp". Colony diameter of control $C = 90$ mm.

Complexes	Different conc^n (ppm) of the complexes	Colony diameter (in mm) at different concentration	% Inhibition $I = [(C–T)/C] \times 100$ at different conc^n (ppm)
p-NO_2PhO-Zn-t(p-Cl)PP	100	58.5	35
	200	39.37	56.2
	300	28.6	68
2,4-Cl_2PhO-Zn-t(pCl)PP	100	57.8	35.7
	200	47.2	47.5
	300	45.2	49.72
p-NH_2PhO-Zn-t(p-Cl)PP	100	53.2	40.83
	200	43	52.22
	300	41.2	54.16
o-NH_2Py-Zn-t(p-Cl)PP	100	57.2	36.4
	200	55	38.8
	300	48.5	46.1

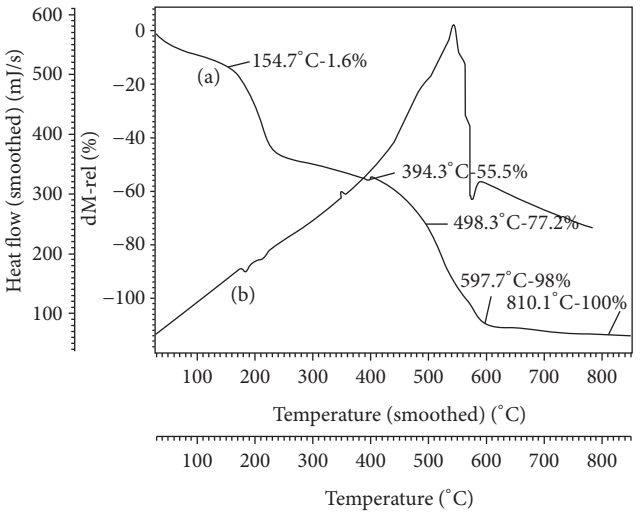

Figure 6: TG curve (a) and DTA curve (b) of o-NH_2phO-Zn-t(p-Cl)PP.

The spectra obtained were used to identify the molecular ion peak formed by the complex.

3.6. Thermal Analysis (TGA/DTA Studies). Thermogravimetric analyses were performed in an air atmosphere at a heating rate of 10°C/min to examine thermal stability of the compound. The TG curve of o-NH_2PhO-Zn-t(p-Cl)PP (Figure 6) show a continuous weight loss starting from 100 to 800°C, when a stable oxide of ZnO is formed. The TG curve shows an initial weight loss due to loss of one amino (–NH_2) moiety up to temperature 154.7°C (observed weight loss = 1.6%, calculated weight loss = 1.72%). This is followed by a steady loss of 55.5% due to loss of the meso-chloro-phenyl groups up to temperature of 394.3°C (calculated weight loss = 55.4%). At 498°C, about 77.2% of the total mass had been lost; corresponding to the collapse of macrocyclic ligand. Simultaneously, there were three exothermal peaks at 340, 540, and 585°C on the DTA curve, corresponding to the decomposition of ligand (H_2-t(p-Cl)PP) (300°C–600°C). The small exothermic peak at 340°C correspond to the loss of chains whereas large exothermic peak at 540°C resulting into total loss of the porphyrin ring skeleton.

3.7. Biological Evaluation

3.7.1. Antifungal Studies. *In vitro* antifungal activity of some of the investigated compounds were tested by agar plate technique [38] against the Pathogen *"Fusarium spp"* by the poisoned food method using Potato Dextrose Agar (PDA) (glucose 20 g, starch 20 g, agar-agar 20 g in 1000 mL distilled water) nutrient as the medium [39]. Solution of the test compounds in DMSO (100, 200, and 300 ppm concentrations) were prepared and mixed with the PDA. The medium was then poured into sterilized Petri-Plates and the spores of fungi were placed on the medium with the help of inoculum's needle inside laminar flow. The plates were inoculated with seven days old culture of the pathogen by placing 2 mm bit of the compound under investigation with different concentration in the centre of plates. The inoculated plates were incubated at 27°C for 5 days. The linear growth of fungus in control and treatment were recorded at different concentrations of the complexes after 5 days. The growth of "Fusarium spp" over control was calculated as

$$\%\ \text{inhibition}\ (I) = \frac{(C - T)/C}{100}, \tag{4}$$

where I = percent inhibition, C = mean growth of fungus in (mm) in control, and T = mean growth of fungus in (mm) in treatment.

Table 7 shows that on increasing the concentration of the complex, the colony diameter of the fungus decreases and hence percent inhibition increases. On increasing the concentration of the complex, the percent inhibition also

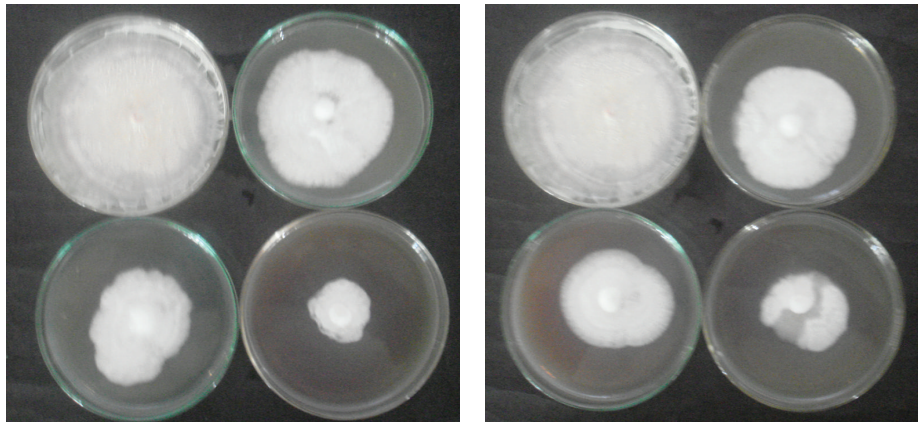

(a) (b)

Figure 7: (a) Antifungal activity of p-NH_2py-Zn-t(p-Cl)PP. (b) Anti-fungal activity of p-NH_2phO-Zn-t(p-Cl)PP.

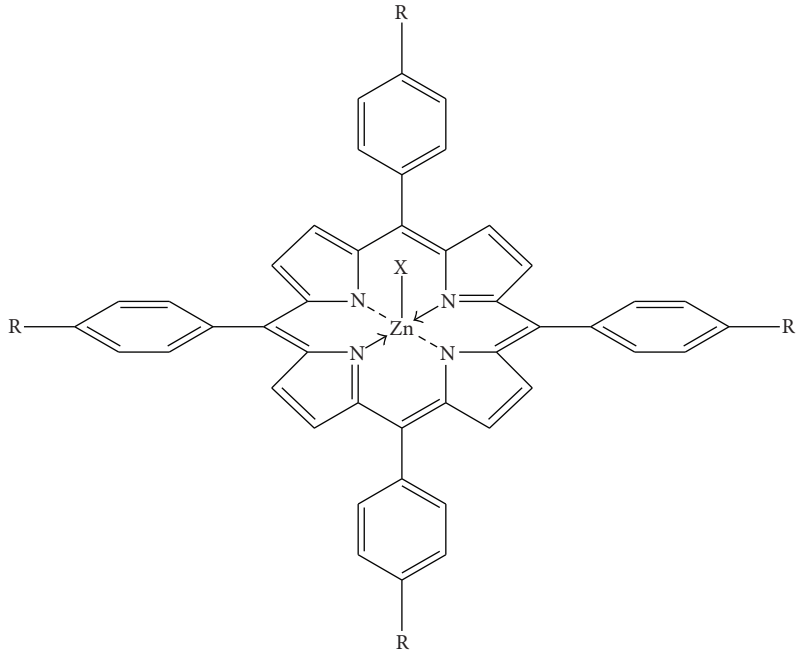

X = different phenolates and pyridinates as axial ligands
R = – H, – Cl

Scheme 1: Proposed structure of axially ligated zinc(II) porphyrins.

increases, which shows linear relationship between concentration and percent inhibition. The increase in the antimicrobial activity is due to faster diffusion of metal complexes as a whole through the cell membrane or due to combined activity effect of the metal, the axial ligand, and the macrocyclic porphyrin ligand. Such increased activity of the metal complexes can be explained on the basis of Overtone's Concept [40] and the Tweedy's chelation theory [41]. The variation in the effectiveness of different complexes against the pathogen depends either on the impermeability of the cell membrane that surrounds the cell favours the passage of only lipid soluble materials due to that liphophilicity is an important factor to control the antimicrobial activity. On chelation, the polarity of the metal ion will be reduced to a greater extent due to overlap of the ligand orbital and partial sharing of the positive charge of the metal ion with donor groups. Antifungal activity of o-NH_2py-Zn-t(p-Cl)PP and p-NH_2phO-Zn-t(p-Cl)PP are displayed in Figures 7(a) and 7(b).

4. Conclusion

On the basis of physicochemical and spectral evidences it is found that all the complexes with a general formula X-Zn^{II}-t(p-Cl)PP (X = different phenolates and pyridinates) in which the four coordinate zinc porphyrin will accept one and only

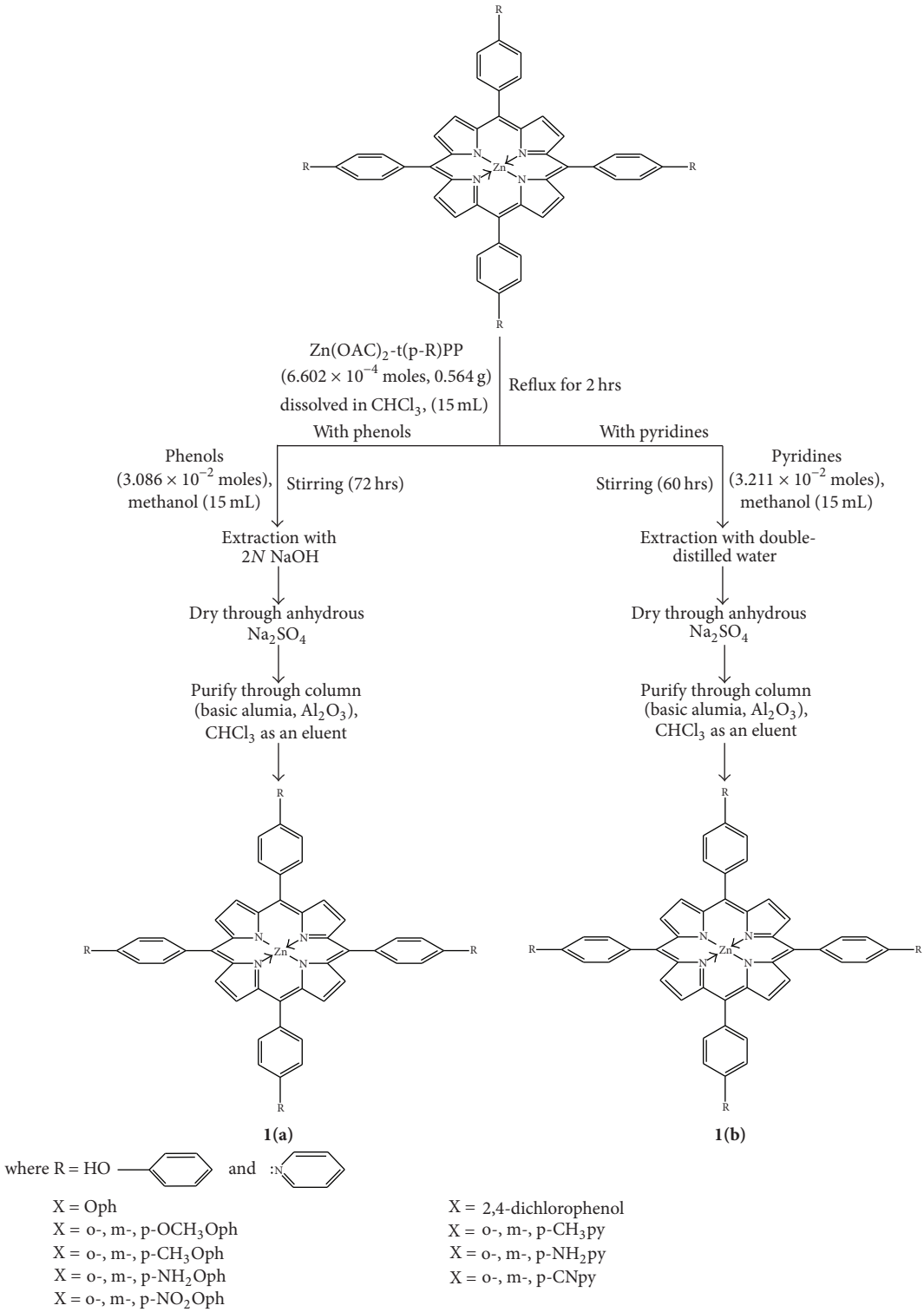

Scheme 2: General scheme for the preparation of 5,10,15,20-meso-tetra(p-chlorophenyl)porphyrin zinc(II) containing different phenolates and pyridinates as axial ligand.

one axial ligand in 1 : 1 molar ratio to form five coordinated complexes. The proposed structure for the complexes under investigation with general formula [X-Zn-t(p-Cl)PP] is given as Scheme 1.

References

[1] S. Banfi, E. Caruso, S. Caprioli et al., "Photodynamic effects of porphyrin and chlorin photosensitizers in human colon

adenocarcinoma cells," *Bioorganic and Medicinal Chemistry*, vol. 12, no. 18, pp. 4853–4860, 2004.

[2] T. E. O. Screen, J. R. G. Thorne, R. G. Denning, D. G. Bucknall, and H. L. Anderson, "Amplified optical nonlinearity in a self-assembled double-strand conjugated porphyrin polymer ladder," *Journal of the American Chemical Society*, vol. 124, no. 33, pp. 9712–9713, 2002.

[3] T. E. O. Screen, J. R. G. Thorne, R. G. Denning, D. G. Bicknall, and H. L. Anderson, "Two methods for amplifying the optical nonlinearity of a conjugated porphyrin polymer: transmetallation and self-assembly," *Journal of Materials Chemistry*, vol. 13, pp. 2796–2808, 2003.

[4] K. Pgawa, A. Ohashi, Y. Kobrke, K. Kamada, and K. Ohta, "Strong two-photon absorption of self-assembled butadiyne-linked bisporphyrin," *Journal of the American Chemical Society*, vol. 125, no. 44, pp. 13356–13357, 2003.

[5] M. Drobizhev, Y. Stepanenko, Y. Dzenis et al., "Understanding strong two-photon absorption in π-conjugated porphyrin dimers via double-resonance enhancement in a three-level model," *Journal of the American Chemical Society*, vol. 126, no. 47, pp. 15352–15353, 2004.

[6] J. L. Humphrey and D. Kuciarskas, "Charge transfer enhances two-photon absorption in transition metal porphyrins," *Journal of the American Chemical Society*, vol. 128, no. 12, pp. 3902–3903, 2006.

[7] J. Chen, W. Zhang, D. Officer, G. F. Swiegers, and G. G. Wallace, "A readily-prepared, convergent, oxygen reduction electrocatalyst," *Chemical Communications*, no. 32, pp. 3353–3355, 2007.

[8] M. S. Choi, T. Yamazaki, I. Yamazaki, and T. Aida, "Bioinspired molecular design of light-harvesting multiporphyrin arrays," *Angewandte Chemie*, vol. 43, no. 2, pp. 150–158, 2003.

[9] A. R. Battersby and E. Mac Donald, "Review of biosyntheses of porphyrins and chlorins," in *Porphyrins and Metalloporphyrins*, K. M. Smith, Ed., Elsevier, Amsterdam, The Netherlands, 1975.

[10] K. M. Kadish, K. M. Smith, and R. Guilard, *The Porphyrin Handbook*, vol. 14, Academic Press, New York, NY, USA, 2000.

[11] N. G. Egger, M. Motamedi, M. Pow-Sang, E. Orihuela, and K. E. Anderson, "Accumulation of porphyrins in plasma and tissues of dogs after δ-aminolevulinic acid administration: implications for photodynamic therapy," *Pharmacology*, vol. 52, no. 6, pp. 362–370, 1996.

[12] S. Nakjima, I. Sokaka, and T. Takemura, "Mechanism of accumulation of porphyrin derivatives in tumor tissues and its application to the diagnosis and treatment of cancer," *Drug Delivery System*, vol. 11, no. 2, pp. 105–110, 1996.

[13] D. Dolphin, T. G. Traylor, and L. Y. Xie, "Polyhaloporphyrins: unusual ligands for metals and metal-catalyzed oxidations," *Accounts of Chemical Research*, vol. 30, no. 6, pp. 251–259, 1997.

[14] W. Su, T. M. Copper, and M. C. Brant, "Investigation of reverse-saturable absorption in brominated porphyrins," *Chemistry of Materials*, vol. 10, no. 5, pp. 1212–1213, 1998.

[15] P. J. Scherer and S. F. Fischer, "Quantum treatment of the optical spectra and the initial electron transfer process within the reaction center of *Rhodopseudomonas viridis*," *Chemical Physics*, vol. 131, no. 1, pp. 115–127, 1989.

[16] K. M. Kadish, K. M. Smith, and R. Guilard, *The Porphyrin Handbook*, Academic Press, San Diego, Calif, USA, 2000.

[17] A. Robertson and S. Shinkai, "Cooperative binding in selective sensors, catalysts and actuators," *Coordination Chemistry Reviews*, vol. 205, no. 1, pp. 157–199, 2000.

[18] X.-B. Peng, J. W. Huang, T. Li, and L.-N. Ji, "Molecular recognition of amino acid esters by porphyrinatozinc(II): observation of a new binding mode," *Inorganica Chimica Acta*, vol. 305, no. 2, pp. 111–117, 2000.

[19] G. R. Deviprasad and F. D'Souza, "Molecular recognition directed porphyrin chemosensor for selective detection of nicotine and cotinine," *Journal of the Chemical Society, Chemical Communications*, no. 19, pp. 1915–1916, 2000.

[20] K. Chichak and N. R. Branda, "Self-assembly of a linear multicomponent porphyrin array through axial coordination," *Chemical Communications*, no. 6, pp. 523–524, 1999.

[21] V. F. Slagt, P. W. N. M. Van Leeuwen, and J. N. H. Reek, "Bidentate ligands formed by self-assembly," *Chemical Communications*, vol. 9, no. 19, pp. 2474–2475, 2003.

[22] V. F. Slagt, M. Röder, P. C. J. Kamer, P. W. N. M. Van Leeuwen, and J. N. H. Reek, "Supraphos: a supramolecular strategy to prepare bidentate ligands," *Journal of the American Chemical Society*, vol. 126, no. 13, pp. 4056–4057, 2004.

[23] O. Q. Munro and H. M. Marques, "Heme–peptide models for hemoproteins. 1. Solution chemistry of *N*-acetylmicroperoxidase-8," *Inorganic Chemistry*, vol. 35, no. 13, pp. 3752–3767, 1996.

[24] K. Ichimori, H. Ohya-Nishoiigughi, and N. Hirota, "A systematic investigation of the effects of axial ligands and peripheral substituents on the electronic structures of Zinc(II) tetraphenylporphyrin π-cation radicals: electrochemical EPR and spectroscopic observation," *Bulletin of the Chemical Society of Japan*, vol. 61, no. 8, pp. 2753–2762, 1988.

[25] C. M. Barzilay, S. A. Sibilia, T. G. Spiro, and Z. Gross, "Elucidation of factors affecting the electronic structures of magnesium(II) and Zinc(II) tetraarylporphyrin radical cations," *Chemistry*, vol. 1, no. 4, pp. 222–231, 1995.

[26] C.-Y. Chem, S.-H. Cheng, and Y. O. Su, "Electrocatalytic oxidation of styrene by a high valent ruthenium porphyrin cation radical," *Journal of Electroanalytical Chemistry*, vol. 487, no. 1, pp. 51–56, 2000.

[27] J. R. Platt and H. B. Klevens, "Spectroscopy of organic molecules in the vacuum ultraviolet," *Reviews of Modern Physics*, vol. 16, no. 3-4, pp. 182–223, 1944.

[28] A. D. Adler, F. R. Longo, J. D. Finarelli, J. Goldmacher, J. Assour, and L. Korsakoff, "A simplified synthesis for meso-tetraphenylporphin," *Journal of Organic Chemistry*, vol. 32, no. 2, pp. 476–487, 1967.

[29] L. Xiangqing, W. Xingqiao, S. Yingyan, G. Jingfu, D. Jiangwen, and L. Guofa, "Separation and Confirmation of matrix materials in logic gate circuit," *Chemical Journal on Internet*, vol. 3, no. 8, pp. 37–38, 2001.

[30] Z. Jing, G. Yang, C. Shaokui et al., "A modified adler method for the synthesis of meso-hydroxyl substituted tetraphenylporphyrins," *Chemical Journal on Internet*, vol. 4, no. 8, pp. 39–42, 2002.

[31] R. M. Silverstein, G. C. Bassler, and T. C. Morrill, in *Spectrometric Identification of Organic Compounds*, John Wiley & Sons, New York, NY, USA, 1991.

[32] J. T. Kloprogge and R. L. Frost, "Raman microscopy study of basic aluminum sulfate. Part II. Raman microscopy at 77 K," *Journal of Materials Science*, vol. 34, no. 18, pp. 4367–4374, 1999.

[33] H. Scheer and J. J. Katz, "Nuclear magnetic resonance spectroscopy of porphyrins and metalloporphyrins," in *Porphyrins and Metalloporphyrin*, K. M. Smith, Ed., p. 399, Elsevier, Amesterdam, The Netherlands, 1975.

[34] G. P. Gurinovich, A. N. Sevchenko, and K. N. Solovyev, in *Spectroscopy of Chlorophyll and Allied Compounds*, Nauka i Tekhnika, Minsk, Russia, 1968.

[35] D. F. Mauch and L. M. Mink, "Microscale synthesis and electronic absorption spectroscopy of tetraphenylporphyrin H_2(TPP) and metalloporphyrins ZnII(TPP) and NiII(TPP)," *Journal of Chemical Education*, vol. 73, no. 12, p. 1188, 1996.

[36] M. Gouterman, in *The Porphyrin*, D. Dolphin, Ed., vol. 3, pp. 1–165, Academic Press, New York, NY, USA, 1978.

[37] R. C. Dougherty, in *Biochemical Application of Mass Spectroscopy*, G. R. Waller, Ed., p. 591, John Wiley & Sons, New York, NY, USA, 1972.

[38] N. Fahmi, C. Saxena, and R. V. Singh, "Spectroscopic characterization and biological potential of palladium(II) complexes of benzylidenehydrazinecarboxamide or -carbothioamide," *Bulletin of the Chemical Society of Japan*, vol. 69, no. 4, pp. 963–969, 1996.

[39] J. M. Vincent, "Distortion of fungal hyphæ in the presence of certain inhibitors," *Nature*, vol. 159, no. 4051, p. 850, 1947.

[40] N. Dharamuaj, P. Viswanathamurthi, and K. Natarajan, "Ruthenium(II) complexes containing bidentate Schiff bases and their antifungal activity," *Transition Metal Chemistry*, vol. 26, no. 1-2, pp. 105–109, 2001.

[41] L. Mishra and V. K. Singh, "Co(ll), Ni(ll) and Cu(lI) and Zn(lI) complexes with Schiff bases derived from 2-aminobenzimidazoles and pyrazolycarboxaldehyde," *Indian Journal of Chemistry*, vol. 32, p. 446, 1993.